Proceedings of the ASME Turbo Expo 2021
Turbomachinery Technical Conference and Exposition
GT2021
June 7 – 11, 2021, Virtual, Online

GT2021-58964

STUDY OF OIL FILM HEAT TRANSFER IN GAS TURBINE ENGINE BEARING CHAMBER

Illia Petukhov, Taras Mykhailenko, Oleksii Lysytsia, Artem Kovalov

National Aerospace University "Kharkiv Aviation Institute", Kharkiv, Ukraine
Email: t.mykhailenko@khai.edu

ABSTRACT

A clear understanding of the heat transfer processes in a gas turbine engine bearing chamber at the design stage makes it possible to properly design the lubrication and sealing systems and ensure the future bearing safe operation. The heat transfer coefficient (HTC) calculated based on the classical Newton-Richman equation is widely used to represent the heat transfer data and useful for the thermal resistance analysis. However, this approach is only formally applicable in the case of a two-phase medium. While there is a need to model a two-phase medium, setting the flow core temperature correctly in the Newton-Richman equation is an issue that is analyzed in this study.

The heat from the flow core is transferred to the boundary of the oil film on the bearing chamber walls by an adjacent air and precipitating droplets. The analysis showed that droplet deposition plays a decisive role in this process and significantly intensifies the heat transfer. The main contribution to the thermal resistance of internal heat transfer is provided by the oil film. In this regard, the study considers the issues of the bearing chamber workflow modeling allowing to determine the hydrodynamic parameters of the oil film taking into account air and oil flow rates and shaft revolutions. The study also considers a possibility to apply the thermohydraulic analogy methods for the oil film thermal resistance determination. The study presents practical recommendations for process modeling in the bearing chamber.

Keywords: gas turbine engine, bearing chamber, heat transfer, thermal resistance, multiphase flow, oil film.

NOMENCLATURE

A_{pq}	interphase surface area in the unit of the mixture volume (m^{-1})
c_p	specific heat capacity (J/(kg-K))
d	diameter (m)
$\vec{D}_T, \vec{D}_u$	differential advection terms
$\vec{F}$	external body force (N/m^3)
$\vec{F}_{lift}$	lift force (N/m^3)
$\vec{F}_{td}$	turbulent dispersion force (N/m^3)
$\vec{F}_{vm}$	virtual mass force (N/m^3)
$\vec{F}_{wl}$	wall lubrication force (N/m^3)
$\vec{g}$	gravitational acceleration (m/s^2)
h	enthalpy (J/kg)
h_{ci}	internal heat transfer coefficient ($W/(m^2 \cdot K)$)
k	thermal conductivity coefficient ($W/(m \cdot K)$)
L	latent heat associated with the phase change (J/kg)
$\dot{m}$	mass flow rate (kg/s)
$\dot{m}_{imp}$	mass vaporization or condensation rate ($kg/(s \cdot m^2)$)
$\dot{m}_s$	mass source per unit wall area due to droplet collection ($kg/(s \cdot m^2)$)
$\vec{n}$	normal vector (dimensionless)
p	pressure (Pa)
Q	heat flux (W)
Q_{br}	heat flux generated by the bearing (W)
q, $\vec{q}$	heat flux density (W/m^2)
$\dot{q}_{imp}$	source term due to liquid impingement from the bulk flow to the wall (W/m^2)
$\vec{R}$	interaction force (N/m^3)
Re	Reynolds number (dimensionless)
S	source term ($kg/(s \cdot m^3)$)
T_{nw}	fluid near-wall temperature (K)
T_{wi}	internal wall temperature (K)
T_m	film half depth temperature (K)
T_{mi}	mixture temperature (K)
$\vec{u}$, $\vec{v}$	velocity (m/s)
Y	mass fraction (dimensionless)

Greek Symbols

α	phasic volume fraction (dimensionless)
δ	thickness (m)
Θ	angle (degrees)
μ	dynamic viscosity (Pa s)
ρ	density (kg/m^3)
σ	surface tension (N/m)
$\overline{\overline{\tau}}$	stress-strain tensor (Pa)
ν	kinematic viscosity (m^2/s)
∇_s	surface gradient operator (m^{-1})

Subscripts

a	air
d	droplet
f	oil film
l	oil
mi	mixture
p, q	phases
s	film surface
σ	surface
w	wall

1. INTRODUCTION

During the gas turbine engine development, one of the critical tasks is minimizing power consumption for lubrication, thermal protection, and pressurization of the bearing chamber. A reliable prediction of the thermal and hydraulic processes in the bearing chamber is required at the design stage to solve this task [1]. The high intensity of the heat transfer processes in three-dimensional multiphase flow of variable structure that depends significantly on the engine operating mode explains the complexity of the prediction problem. The behavior of the multiphase flow consisting of oil droplets, oil film, and air is mainly influenced by the oil and airflow rates, bearing shaft rotation speed and direction, bearing chamber design, internal pressure, variation of the thermodynamic properties of the phases due to heat transfer, the chamber wall roughness [2-19].

The gas turbine engine bearing chamber is filled with a mixture of supplied lubricating oil and air that leaks through the seals (see Fig. 1). The oil droplets are generated in the multiphase flow core with a low volume fraction of the liquid as a result of lubricating oil contact with the rotating bearing and shaft (see Fig. 2). The generated oil droplets interact with a swirling airflow and get to the internal chamber wall creating the oil film. The film moves under the influence of shear forces, gravity, and viscosity, as well as under the influence of droplets impact. Oil droplets impingement causes the oil film splashes that generate the secondary droplets, which further interact with the flow core (see Fig. 2). As a result, a transition region is formed near the wall, where oil becomes a continuous phase. Thus, the two-phase flow structure in the near-wall region of the bearing chamber is very complex [2, 13], and the oil film thickness is nonuniform [3-8]. This nonuniformity determines the variability of the oil film thermal resistance that affects the heat transfer processes between the bearing chamber wall and the air-oil mixture [9-12]. In turn, the heat transfer processes affect the temperature state for both the lubrication oil and the bearing chamber elements.

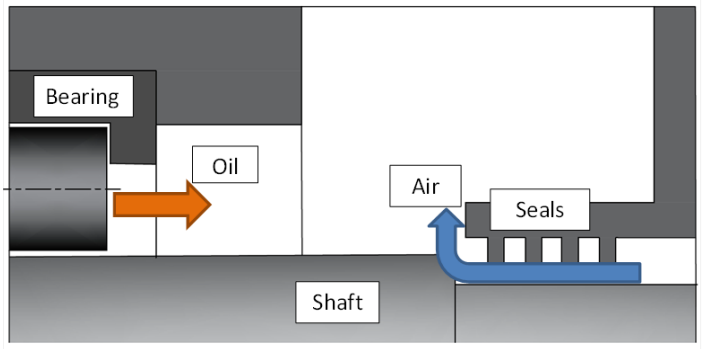

FIGURE 1: SCHEMATIC DIAGRAM OF THE OIL AND AIR FLOWS IN THE COMPACT BEARING CHAMBER

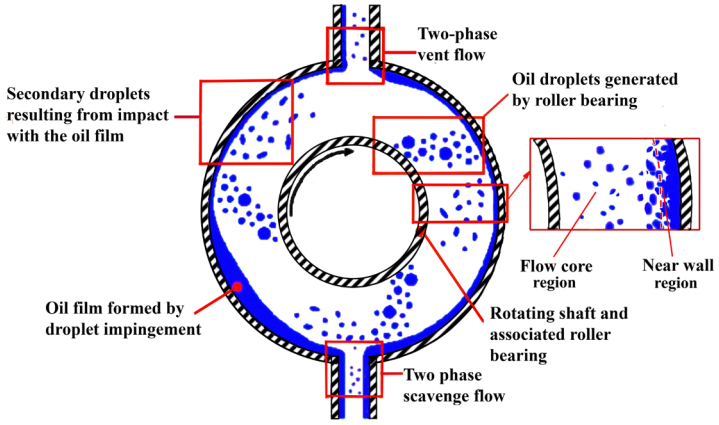

FIGURE 2: MULTIPHASE FLOW STRUCTURE IN THE BEARING CHAMBER [2]

Data on heat transfer in the bearing chamber are essential for lubrication and sealing air systems design. Correct operation of these systems helps avoid the bearing overheating, which may lead to failure, and ensure the lubrication oil's safe temperature conditions. The heat transfer coefficient (HTC) in the bearing chamber determined based on the Newton-Richman law (1) is widely used to represent the heat transfer data.

$$h_{ci} = \frac{q_w}{\left(T_{nw} - T_{wi}\right)}, \quad (1)$$

where T_{nw} is a fluid near-wall temperature, T_{wi} is an internal wall temperature, q_w is a wall heat flux density.

In the case of HTC calculation for a two-phase medium based on experimental data, the correct choice of the temperature that characterizes the T_{nw} temperature is an important and ambiguous issue. In experimental studies [3, 9-

12], either fluid temperature measured at some distance from the chamber wall or scavenge oil temperature is used for this purpose. Such choices made an influence on the HTC values observed in the studies.

The application of modeling methods based on the multiphase flow mechanics and Computational Fluid Dynamics (CFD) enables the prediction of thermal and hydrodynamic processes in the bearing chamber. The problem relevance and modeling approach efficiency are evidenced by studies [13-19]. These methods fundamentally allow taking into account the influence of all factors involved in the mathematical model. However, the ambiguities associated with the oil film behavior modeling, the droplets flow parameters specification, and the interfacial interaction conditions in the wall region complicate the use of existing mathematical models. Therefore, a combination of simulation methods and experimental studies is crucial for understanding the heat transfer and flow distribution phenomena in the bearing chamber.

The presented study contributes to developing a reliable, experimentally validated methodology to analyze the fluid distribution and heat transfer coefficients in different zones of the bearing chamber. This study explores modeling the oil film heat transfer taking into account the engine operation modes to enable reliable heat transfer prediction in the bearing chamber.

2. METHODOLOGY

Heat transfer in the gas turbine engine bearing chamber depends on many factors, like flow structure, shaft rotational speed, amount of injected oil, airflow rate over the labyrinth seal, bearing chamber geometry.

Complications during the simulation of the heat transfer in the bearing chamber are caused by the fluid multiphase nature and the mixture dissimilarity (see Fig. 2), as well as by the interrelation of thermal and hydraulic processes. Such complex behavior does not allow obtaining universal criterion equations or CFD procedures for the HTC determination in the bearing chamber. For these reasons, particularly, the values of local internal HTC (1) reported in different studies [9-12] vary quite noticeably.

Thus, the problem of selecting mathematical models and software modules, and methods of their application and combination still remains relevant for CFD modeling. To make a choice, it is crucial to assess the contribution of individual factors to the heat transfer process. Also, it is necessary to take into account available computation capacities.

Heat transfer from the central part of the chamber (flow core region) to the near-wall region, where oil becomes a continuous medium (Fig. 2), is realized via air motion and droplet deposition. Due to the significant difference in the phase densities, the volume fraction of droplets does not exceed 0.3% in the flow core region, even in the case of equal oil and air flow rates. In this region, the continuous medium is air with a low coefficient of thermal conductivity. Heat transfer by the air convection only gives a heat transfer coefficient less than 150 W/(m^2 K) even at the highest shaft revolutions [20]. It is about an order of magnitude lower than the observed values of internal HTCs [9-12].

Thus, the main contribution to the heat transfer is made by oil droplets that splash from the bearing (Fig. 2). These droplets initially accumulate the energy associated with the bearing heat. While moving towards the chamber wall, the oil droplets interact with air, and their temperature changes. Due to the extended air-droplet interface, the oil droplet heat transfer contribution to the oil temperature changing is much higher than at the air-film interface.

While approaching the wall, the oil droplets form a near-wall region with a high oil concentration (Fig. 2). The temperature of the droplets that deposited in this region determines the temperature T_{nw} in relation (1). Oil becomes a continuous phase here and the mechanisms of interfacial interaction and heat transfer change. Therefore, while modeling, the computation domain should be divided into separate flow core and near-wall regions.

2.1 Flow core processes

The intensity of interphase transfer in the flow core is determined by the sizes of droplets and differences in the phases' temperatures and velocities. Two models can be used to determine the parameters of droplets in the near-wall region: homogeneous and inhomogeneous. The inhomogeneous model allows to determine the parameters more accurately but uses a larger number of equations and boundary conditions as well as requires more powerful computation capacities

Simultaneously, from the heat transfer point of view, thermohydraulic processes in the flow core determine the temperature T_{nw} (1) and the parameters of the near-wall oil film motion, which affect oil film thermal resistance. In all cases, the interphase processes of momentum and energy exchange tend to the equilibrium state. For interphase heat transfer, the equilibrium temperature is the mass average temperature of the phases. For the droplets in the near-wall region, the deviation magnitude from the equilibrium temperature is related to droplets size, and the direction (sign) of deviation is determined by the initial ratio of the air and oil phase temperatures. The deviation values can be obtained only as a result of the inhomogeneous modeling of the multiphase media mechanics. The homogeneous model such as Volume of Fluid (VOF) model gives a mass average temperature only.

Such mass-average temperature can be quite correctly used as the temperature T_{nw} of unperturbed flow near the wall (1) outside of the boundary layer. Moreover, T_{nw} is essential for presenting the numerical simulation results. In this study, the temperature T_{mi} of the oil-air mixture after the bearing was selected as T_{nw} temperature. The T_{mi} temperature of the mixture can be determined by its enthalpy:

$$h_{mi} = h_l Y_l + h_a (1 - Y_l) + Q_{br} / (\dot{m}_l + \dot{m}_a), \qquad (2)$$

where the oil mass fraction is

$$Y_l = \frac{\dot{m}_l}{\dot{m}_l + \dot{m}_a}, \quad (3)$$

where $\dot{m}_l, \dot{m}_a$ are mass flow rates of oil and air, respectively.

The enthalpy of each phase is calculated in accordance with corresponding parameters at the bearing chamber inlet. Since the oil heat capacity depends on the temperature, the method of successive approximations was used to determine the mixture temperature T_{mi} , which is the temperature near the wall T_{nw}, by its enthalpy.

The heat generation in the bearing Q_{br} can be determined for a given geometry of bearing elements, revolutions, and radial load using the methodology similar to those presented in studies [21-23].

Eulerian model

The Eulerian multiphase model realized in ANSYS Fluent [24] allows modeling multiple separate yet interacting phases. An Eulerian treatment is used for each phase. The solution is based on the assumption that a single pressure is shared by all phases *n*, while the conservation equations are solved for each phase.

The description of multiphase flow as interpenetrating continua incorporates the concept of phase volume fractions, denoted here by α_q, with

$$\sum_{q=1}^{n} \alpha_q = 1.$$

With this approach, all values in the conservation equations, including those describing the interphase interaction, are written for a unit volume of the mixture. The continuity equation for q phase is

$$\frac{\partial}{\partial t}(\alpha_q \rho_q) + \nabla \cdot (\alpha_q \rho_q \overrightarrow{v_q}) = \sum (\dot{m}_{pq} - \dot{m}_{qp}) + S_q \quad (4)$$

where $\vec{v}_q$ is a velocity of phase q; $\dot{m}_{pq}$ characterizes the mass transfer from the p^{th} to q^{th} phase; $\dot{m}_{qp}$ characterizes the mass transfer from phase q to phase p; S_q is a source term. In the absence of mass transfer, the right side of equation (4) is equal to zero.

The momentum balance for phase q is

$$\frac{\partial}{\partial t}(\alpha_q \rho_q \overrightarrow{v_q}) + \nabla \cdot (\alpha_q \rho_q \overrightarrow{v_q}\overrightarrow{v_q}) = -\alpha_q \nabla p + \nabla \cdot \overline{\overline{\tau}}_q +$$
$$+ \alpha_q \rho_q \vec{g} + \sum_{p=1}^{n} (\vec{R}_{pq} + \dot{m}_{pq}\vec{v}_{pq} - \dot{m}_{qp}\vec{v}_{qp}) + \quad (5)$$
$$+ (\vec{F}_q + \vec{F}_{lift,q} + \vec{F}_{wl,q} + \vec{F}_{vm,q} + \vec{F}_{td,q})$$

where $\overline{\overline{\tau}}_q$ is a q^{th} phase stress-strain tensor.

Here, $\vec{F}_q$ is an external body force, $\vec{F}_{lift,q}$ is a lift force, $\vec{F}_{wl,q}$ is a wall lubrication force, $\vec{F}_{vm,q}$ is a virtual mass force, and $\vec{F}_{td,q}$ is a turbulent dispersion force, which is used in the case of turbulent flows only. $\vec{R}_{pq}$ is an interaction force between phases, and p is the pressure shared by all phases.

To describe the conservation of energy in Eulerian multiphase application, a separate enthalpy equation can be written for each phase:

$$\frac{\partial}{\partial t}(\alpha_q \rho_q h_q) + \nabla \cdot (\alpha_q \rho_q \overrightarrow{u_q} h_q) =$$
$$= \alpha_q \frac{dp_q}{dt} + \overline{\overline{\tau}}_q : \nabla \vec{u}_q - \nabla \cdot \vec{q}_q + S_q + \quad (6)$$
$$+ \sum_{p=1}^{n} (Q_{pq} + \dot{m}_{pq} h_{pq} - \dot{m}_{qp} h_{qp})$$

where h_q is a specific enthalpy of the q^{th} phase, $\vec{q}_q$ is a heat flux, S_q is a source term that includes sources of enthalpy (for example, due to chemical reaction or radiation), Q_{pq} is an intensity of heat exchange between the p^{th} and q^{th} phases, and h_{pq} is an interphase enthalpy.

Volume of Fluid model

The VOF model considers two or more immiscible fluids by solving a single set of momentum equations and tracking each fluid's volume fraction throughout the domain. In view of the equality of the phase velocities, the continuity equation (4) can be transformed into an equation for its volume fraction as a result of dividing by the phase density.

The single momentum equation (7) is dependent on the volume fractions of all phases through the mixture density ρ and dynamic viscosity μ.

$$\frac{\partial}{\partial t}(\rho \overrightarrow{v}) + \nabla \cdot (\rho \overrightarrow{v}\overrightarrow{v}) =$$
$$= -\nabla p + \nabla \cdot \left[\mu (\nabla \vec{v} + \nabla \vec{v}^{T}) \right] + \rho \vec{g} + \vec{F} \quad (7)$$

Inhomogeneous model

The Ansys CFX implements the inhomogeneous model as a part of the Particle Model, which is designed to describe the behavior of a two-phase flow containing continuous and dispersed phases. Based on Euler's approach, a heterogeneous monodispersed oil-air flow was modeled in the study subject to the condition of the two-phase flow structure inversion in the near-wall region from drip to bubble. As a result, it was

possible to exclude a mathematical model for phase three (the oil film) from consideration.

The proposed approach assumes that one of the phases is continuous (phase *p*) and the other is dispersed (phase *q*). The area of the interphase surface per unit of the mixture volume, known as the interfacial area density, is calculated from the following formula

$$A_{pq} = \frac{6\tilde{\alpha}_q}{d_q} \tag{8}$$

by assuming that the dispersed phase is present as spherical particles of mean diameter d_q.

For model operability in the whole diapason of the volume fractions of the dispersed phase, the limits (α_{max}=0.8, α_{min}=10^{-7}) were imposed, and the area density (8) was defined in accordance with the algorithm:

$$\tilde{\alpha}_q = \begin{Bmatrix} max(\alpha_q, \alpha_{min}) & if & (\alpha_q \le \alpha_{max}) \\ max\left(\frac{1-\alpha_q}{1-\alpha_{max}}\alpha_{max}, \alpha_{min}\right) & if & (\alpha_q > \alpha_{max}) \end{Bmatrix} \tag{9}$$

When the volume fraction α_q of dispersed phase tends to zero, the lower limit of volume fraction α_{min} is used to avoid the convergence problems. In the case of high-volume fraction α_q, there may be a violation of the condition of the *q* phase existence as a dispersed phase, which corresponds to the inversion of the two-phase flow structure. Then, the area density is decreased to reflect that it should lead to zero as α_q tends to 1.

2.2 Near-wall processes

The flow parameters in the near-wall region of the bearing chamber are determined by a combination of the following primary and secondary effects. The primary effects are those associated with the flow core phases impingement with the impermeable wall. The nature of oil and air interaction with the wall is different due to the wall surface wettability and the difference in the inertial properties of the phases. Liquid droplets fall and form a film on the wall, while air generates shear stresses on its surface. Secondary effects are associated with the droplet-film interaction. Droplets impingement causes the oil film turbulization, increases its average velocity, and intensifies the heat transfer. Droplets reflected from the oil film, and those generated by the splashes have a lower velocity during subsequent impingement, thus, later on, provide a lower contribution to the heat transfer processes. Besides, a dense two-phase layer is formed near the surface of a single-phase film. This layer prevents direct interaction between the film and primary droplets that transfer heat from the flow core. The process is further complicated by the flow nonuniformity around the bearing chamber circumference, associated with the gravity influence.

The phenomena mentioned above are associated with hydrodynamic processes, to which a large number of studies and publications are devoted. At the same time, specific difficulties are associated with the implementation of end-to-end counting in the entire chamber space based on a single conceptual model of a two-phase flow because air is a continuous medium in the core, while oil is a continuous medium in the near-wall region. Even when the flow structure inversion condition (9) is used, the wall film single-phase state modeling remains practically unsolvable. Simultaneously, wall film thermal resistance is decisive in the heat transfer process from the flow core to the wall.

Specific progress in this direction is associated with the application of the Eulerian Wall Film (EWF) model. A rational combination of the flow core and film models [15] in a single computational module is of great importance for the problem under analysis. However, in this case, only hydrodynamic problems matter. At the same time, if the accuracy of the EWF-based solution is sufficiently high, it is also possible to analyze the near-wall region thermal resistance structure, including an oil film. The thickness and, therefore, the thermal resistance of the near-wall film decrease in the case of reduction of diameter and increasing of velocity of the oil droplets generated by the bearing. The same effect on the near-wall film characteristics has shear stresses increasing at the boundary of the flow core and film surface, associated with shaft revolution increasing. In turn, the shaft revolution increasing results in increasing of the internal heat transfer coefficient that was noted by many researchers [3, 9, 10, 12].

Eulerian Wall Film model

The EWF model can be used to predict the creation and flow of thin liquid films generated as a result of the liquid drops impingement with a solid wall surface. There are several possible outcomes from the impingement: *stick*, *rebound*, *spread*, and *splash* [24].

Conservation of mass for the film in a 3D domain can be presented in the following way:

$$\frac{\partial \rho_l \delta_f}{\partial t} + \nabla_s \cdot \left(\rho_l \delta_f \vec{u}_f\right) = \dot{m}_s \tag{10}$$

where ρ_l is a liquid density; δ_f is a film thickness; ∇_s is a surface gradient operator; $\vec{u}_f$ is a mean film velocity; $\dot{m}_s$ is a mass source per unit wall area due to droplet collection.

Conservation of the film momentum can be written as:

$$\begin{aligned} &\frac{\partial \rho_l \delta_f \vec{u}_f}{\partial t} + \nabla_s \cdot \left(\rho_l \delta_f \vec{u}_f \vec{u}_f + \vec{D}_u\right) = \\ &= -\delta_f \nabla_s p_L + \rho_l \delta_f \vec{g}_\tau + \frac{3}{2}\vec{\tau}_{fs} - \frac{3\mu_l}{\delta_f}\vec{u}_f + \dot{\vec{q}}_s + \vec{\tau}_{\partial w} \end{aligned} \tag{11}$$

where

$$p_L = p_a + p_\delta + p_\sigma \,, \tag{12}$$

$$p_\delta = -\rho_l \delta_f (\vec{n} \cdot \vec{g}) \,, \tag{13}$$

$$p_\sigma = -\sigma \nabla_s \cdot (\nabla_s \delta_f) \,. \tag{14}$$

The momentum source term due to droplet collection has a form of:

$$\dot{\vec{q}}_s = \dot{m}_s (\vec{u}_d - \vec{u}_f) \,. \tag{15}$$

Conservation of film energy can be given as:

$$\frac{\partial \rho_l \delta_f T_f}{\partial t} + \nabla_s \cdot \left(\rho_l \delta_f T_f \vec{u}_f + \vec{D}_T \right) = \\ = \frac{1}{C_p} \left[\frac{2k_f}{\delta} \left(T_s + T_{wi} - T_m \right) + \dot{q}_{imp} + \dot{m}_{imp} L \right], \tag{16}$$

where T_f is an average film temperature; $\vec{D}_T$ is a differential advection term; k_f is a thermal conductivity; T_s is a film surface temperature; T_{wi} is an internal wall temperature; T_m is a film half depth temperature; $\dot{q}_{imp}$ is a source term due to liquid impingement from the bulk flow to the wall; $\dot{m}_{imp}$ is a mass vaporization or condensation rate and L is a latent heat associated with the phase change.

The EWF model assumes that the film properties do not vary over the film thickness and that the film is thin enough so that the liquid flow in the film can be considered parallel to the wall. At the same time, the equation of film energy conservation (16) contains the film half depth temperature T_m, which can be used to take into account temperature changes over the film thickness. The most comfortable case for such changes accounting is a laminar film with a velocity profile linear over the thickness. This approach, for example, is implemented for the Shear-Driven Film model [24]. In this case, the temperature changes according to the linear law also. Moreover, for a constant thickness film, the adjacent flow velocity variation changes the velocity on its free surface. However, it does not affect the temperature gradient that determines the heat transfer.

Thermohydraulic processes in the flow core (see Fig. 2) determine the temperature T_{nw} of undisturbed flow adjacent to the film surface. This temperature is close to the mass-average temperature T_{mi} of the flow core, determined by the enthalpy (2). Therefore, the value of the internal heat transfer coefficient (1) is determined only by the thermal resistance of the wall oil film. In this case, for laminar film

$$h_{ci} = \frac{k_o}{\delta_f} \,. \tag{17}$$

The laminar regime for thin films is maintained at the Reynolds number (18) less than 400.

$$Re_f = \frac{\delta_f \cdot u_f}{\nu_f} \,, \tag{18}$$

Moreover, for Reynolds numbers less than 50, the shear film flow is not accompanied by the wave formation [25].

3. RESULTS AND DISCUSSION

Some experimental data are generally needed to validate any new CFD modeling approach. The studies [9-10] contain experimental data on heat transfer in the bearing chambers. For numerical and experimental results comparison within this study, a bearing chamber II was selected, and a relevant computation domain was created. Details of boundary conditions are represented in Fig. 3. A mesh of 2 million elements consisting of tetra and hexa elements (Fig. 4) was selected based on the mesh convergence study.

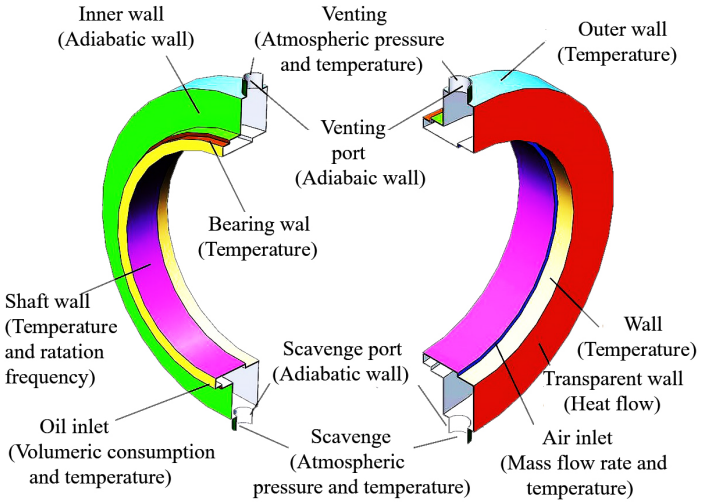

FIGURE 3: BOUNDARY CONDITIONS FOR THE BEARING CHAMBER

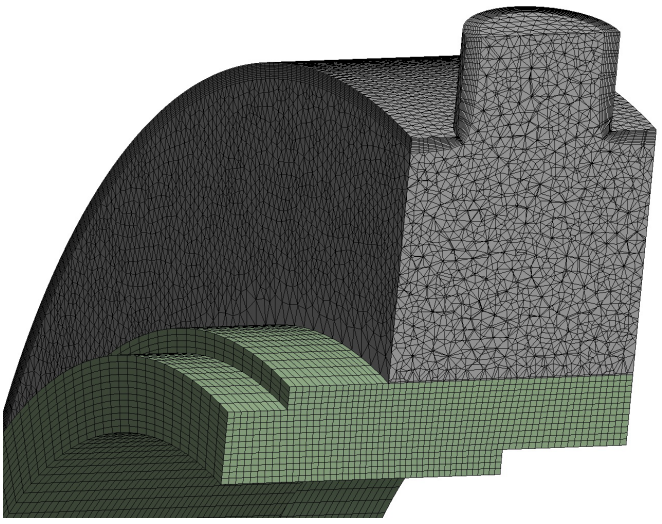

FIGURE 4: MESH FOR THE BEARING CHAMBER

CFD modeling of the bearing chamber processes was carried out for the following gas turbine engine operation conditions: rotation speed – 9000 rpm, air mass flow rate – 0.015 kg/s, oil flow rate – 0.012 kg/s.

To solve this problem, the following main settings were used: a Pressure Based Transient solver with a variable time step of 10^{-6} ... 10^{-5} s; Pressure-Velocity coupling method; Coupled with volume fractions scheme; Green-Gauss node based gradient, Compressive volume fraction and PRESTO pressure discretization.

For Eulerian multiphase model the following main settings were used: Turbulent model "k-ω SST" for per phase; viscous heating; curvature correction options; implicit volume fraction parameters; surface tension force modeling; continuum surface force; wall adhesion options; Shiller-Nauman drag coefficient for Eulerian multiphase model.

For VOF model the following main settings were used: Turbulent models "k- ω SST"; implicit volume fraction parameters; implicit body force formulation; turbulence damping; curvature correction and production limiter options.

The results obtained using the flow structure inversion approach (Ansys CFX) indicate a non-uniform distribution of the oil volume fraction in the bearing chamber (Fig. 5), which influences the heat transfer coefficient value (Fig. 6). However, this approach assesses the oil film distribution on the chamber wall indirectly. The heat transfer in the near-wall region is determined based on the multiphase flow structure inversion algorithm (9). It is mainly caused by the interaction of droplets with the wall surface. In this case, the actual single-phase oil film is not described, and there is an uncertainty associated with the determination of the volume fraction α_{max}, at which the structure inversion occurs.

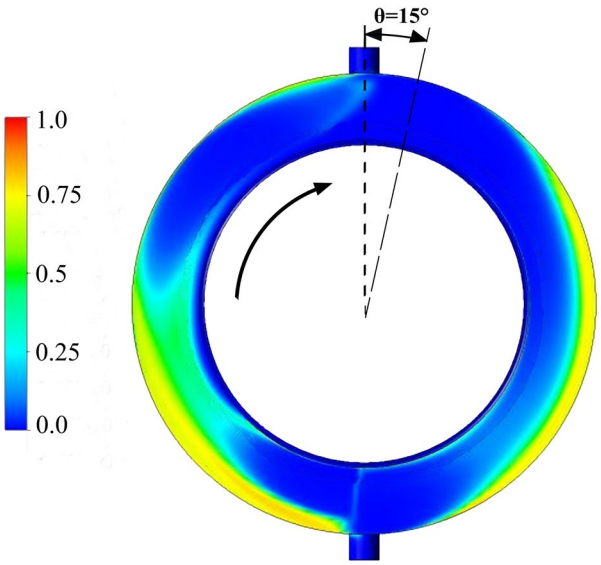

FIGURE 5: OIL VOLUME FRACTION DISTRIBUTION IN THE BEARING CHAMBER

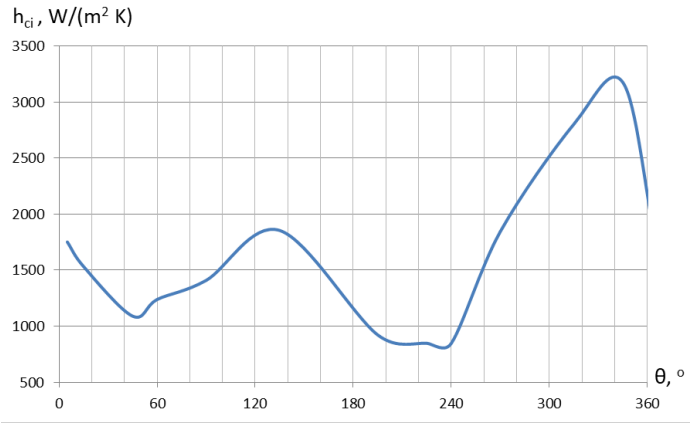

FIGURE 6: HEAT TRANSFER COEFFICIENT AROUND THE BEARING CHAMBER CIRCUMFERENCE

The Eulerian model application (ANSYS Fluent) allows determining the parameters of each phase separately, as shown in Fig. 7-9. In turn, the VOF model (ANSYS Fluent) determines the parameters of the oil-air mixture (Fig. 10 - 11).

FIGURE 7: OIL PATHLINES IN THE BEARING CHAMBER

FIGURE 8: AIR TEMPERATURE CONTOURS (K) IN THE BEARING CHAMBER FOR ANGLE CUT Θ = 15^{O}

FIGURE 9: OIL TEMPERATURE CONTOURS (K) IN THE BEARING CHAMBER FOR ANGLE CUT Θ = 15^{O}

FIGURE 10: MIXTURE TEMPERATURE CONTOURS (K) IN THE BEARING CHAMBER FOR ANGLE CUT Θ = 15^{O}

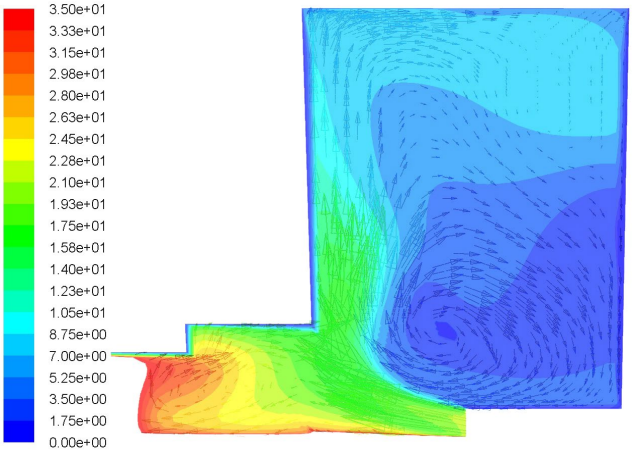

FIGURE 11: MIXTURE VELOCITY (m/s) IN THE BEARING CHAMBER FOR ANGLE CUT Θ = 15^{O}

The Eulerian and VOF models gave similar results when simulating processes in the bearing chamber, where the droplets in the flow core are about 30 μm. However, for a given problem, the average computation time in the case of the Eulerian model application was almost two times higher than in the case of the VOF model application.

The EWF model ANSYS Fluent) allows taking into account the peculiarities of the transition from a two-phase flow in the flow core to a single-phase oil film on the chamber walls. Figure 12 compares the CFD modeling results obtained by using VOF (flow core region) and EWF (near-wall region) models with experimental data of Kurz W. et al. [6].

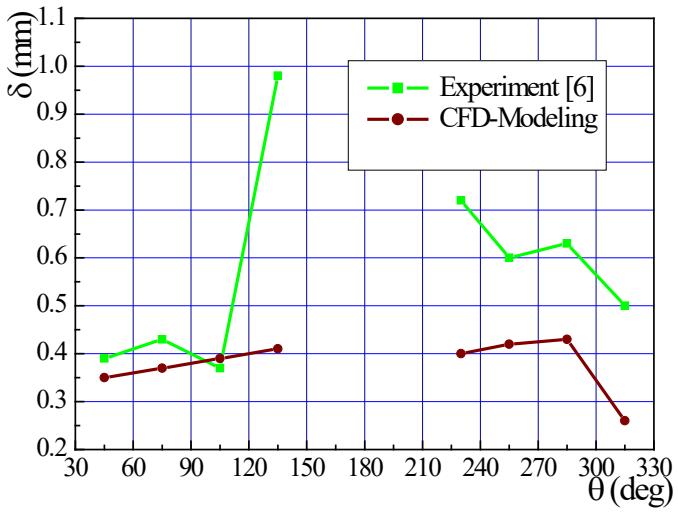

FIGURE 12: DISTRIBUTION OF OIL FILM THICKNESS OVER THE CHAMBER CROSS-SECTIONS

The difference is observed in the 135º section. A similar difference between calculations and experiments in 135º section is also observed in [16]. It can be explained by peculiarities of the film thickness measurements during the experimental studies. Therefore, the EWF and VOF models can be used to

describe oil film parameters from the hydrodynamic point of view, but the problem of the heat transfer description in the near-wall region remains relevant.

According to the calculated results (Fig. 13), the oil film thickness varies along the circumference of the chamber from 0.3 to 0.6 mm (in general). The velocity of the film motion (Fig. 14) is determined by the momentum of precipitating droplets, gravity and shear force at the film-air interphase, as well as by the surface friction. Basically, the velocity does not exceed 1 m/s. For such modes, the Reynolds number (18) does not exceed 250. The level of the heat transfer coefficient (17) is 250-700 W/(m^2 K) with an increase up to 1200-1500 W/(m^2 K) in the regions of the thinnest film.

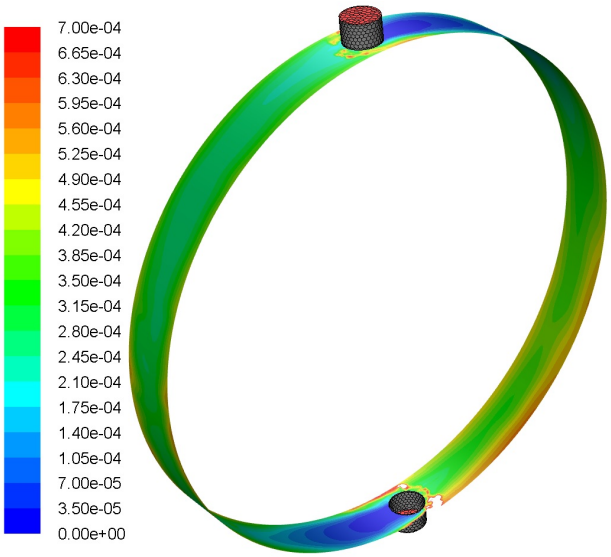

FIGURE 13: OIL FILM THICKNESS (m) ON THE BEARING CHAMBER WALL

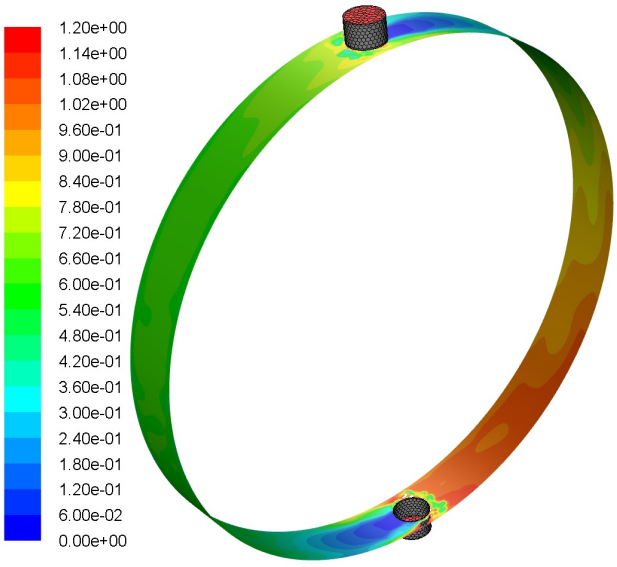

FIGURE 14: OIL FILM VELOCITY (m/s)

The obtained results contribute to developing an experimentally-validated methodology to analyze the fluid distribution and heat transfer in the bearing chamber. The flowchart (Fig. 15) shows the further steps that involve the experimental study of bearing chamber workflow under various operation conditions. Data accumulated during experimental studies will be further used to refine the CFD model.

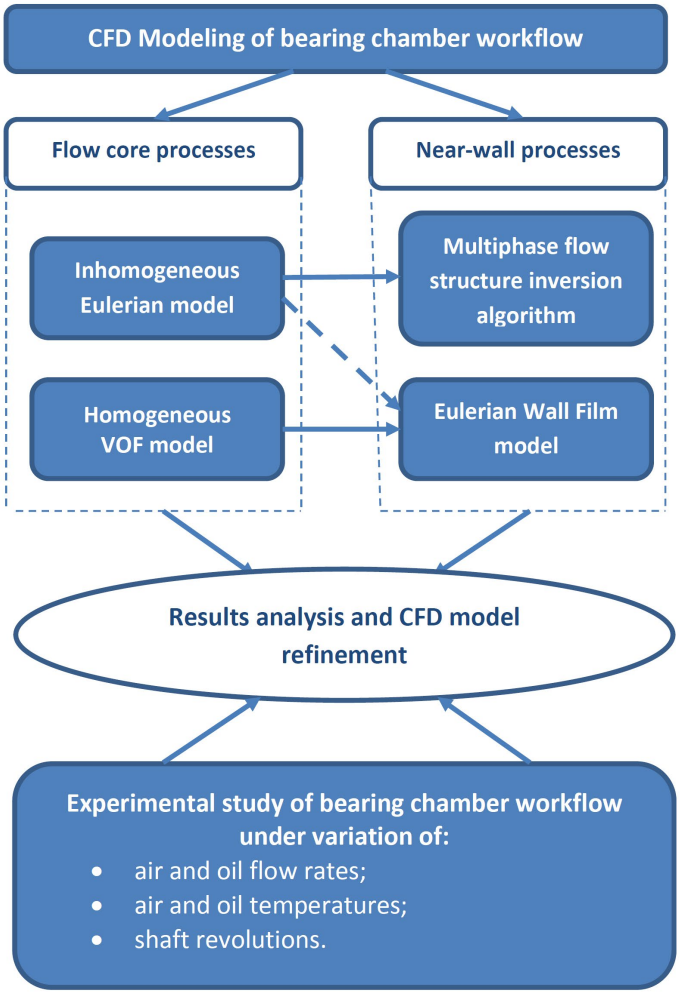

FIGURE 15: FLOWCHART OF BEARING CHAMBER WORKFLOW ANALYSIS

4. CONCLUSION

Two regions in the bearing chamber volume should be distinguished: a flow core with a gas-droplet structure and a near-wall region, where a liquid becomes a continuous phase (Fig. 2). Any mathematical model of the workflow should ensure the continuous transition from one structure to another during numerical implementation. Subject to this provision, both homogeneous and inhomogeneous multiphase models can be used.

The inhomogeneous model (e.g., Inhomogeneous model in Ansys CFX or Eulerian model in Ansys Fluent) allows taking into account the differences in the phases' temperatures and velocities, as well as considering the oil droplet diameter influence on the heat transfer process. However, the form of the equations in the description of interphase interaction depends on the flow structure. Therefore, it is necessary to use the flow structure inversion condition when switching from the flow core to the near-wall region.

The homogeneous VOF model uses fewer equations and does not require their correction when switching from the flow core to the near-wall region. Also, the boundary condition matrix is simpler and the calculation time is lower compared to the inhomogeneous model. However, the reliability of calculation decreases in case of significant contribution of the interphase interaction effects on heat transfer, i.e. in case of large droplet presence.

For both models, it isn't easy to model the workflow directly at the wall surface. Certain progress in modeling of the near-wall region processes is associated with the application of the EWF model, which allows to model separately the near-wall region. A rational combination of the flow core and film models in a single computational module is of great importance for such complex problem solving. The combination of VOF and EWF models is promising for analysis of the heat transfer processes in the gas turbine engine bearing chamber from the point of view of results reliability and computational resources saving.

Additional progress in near-wall region processes modeling can be achieved thanks to separate analysis of hydrodynamic and thermal processes while taking into account the interdependence of the critical effects. The performed analysis shows that the film thermal resistance plays a decisive role in the heat transfer process. Droplets transfer heat from the flow core to the near-wall region, while the air mainly contribute to interphase heat transfer during the droplet motion.

Since any interfacial processes tend to an equilibrium, the droplets' maximum temperature is the mass-average temperature of the mixture T_{mi} determined by relation (2). The indicated mass-average temperature can be used as the undisturbed flow temperature T_{nw} to determine the heat transfer coefficient (1) in the bearing chamber. The magnitude of deviation from this temperature depends on the droplet size, while the deviation sign depends on the initial phase temperature ratio. The homogeneous model, for example, the VOF model, directly calculates the mass-average temperature at the boundary of the near-wall region.

The oil film parameters obtained from the EWF model make it possible to determine its thermal resistance. In many cases, the film can be considered as laminar and the HTC can be determined by the relation (17). For the turbulent regime of film motion, its thermal resistance can be determined by using the similarity methods for thermal and hydrodynamic boundary layers.

The proposed approach for modeling the oil film heat transfer makes it possible to calculate the local value of HTC (1) using the data on the oil film velocity and thickness resulted from the CFD modeling of the isothermal (without heat transfer) process in the bearing chamber. Besides, performed studies and achieved results substantiated the possibility of using the mass-average temperature T_{mi} determined by relation (2) as the undisturbed flow temperature T_{nw} for the local heat flux density calculation. Also, an analysis of the factors that influence the accuracy of the T_{mi} temperature determination was performed.

ACKNOWLEDGEMENTS

The research leading to these results has been performed in the frame of the "Advanced Modeling Methodology for Bearing Chamber in Hot Environment (AMBEC)" project. This project has received funding from the Clean Sky 2 Joint Undertaking under the European Union's Horizon 2020 research and innovation program under grant agreement No 785493.

REFERENCES

[1] Klingsporn, M., 2004, "Advanced Transmission and Oil System Concepts for Modern Aero-Engines", Proceedings of ASME Turbo Expo 2004, Vienna, Austria, June 2004, GT2004-53578.

[2] Wang, C., Morvan, H. P., Hibberd, S. and Cliffe, K. A., 2011, "Thin Film Modeling for Aero-Engine Bearing Chambers", Proceedings of ASME Turbo Expo 2011, Vancouver, British Columbia, Canada, June 2011, GT2011-46259.

[3] Wittig, S., Glahn, A., and Himmelsbach, J., 1994, ''Influence of High Rotational Speeds on Heat Transfer and Oil Film Thickness in Aero Engine Bearing Chambers,'' ASME Journal of Engineering for Gas Turbines and Power, 116 (2), pp. 395-401.

[4] Glahn, A. and Wittig, S., 1996; "Two-Phase Air/Oil Flow in Aero Engine Bearing Chambers: Characterization of Oil Film Flow", ASME Journal of Engineering for Gas Turbines and Power, 118(3), pp. 578-583.

[5] Gorse, P., Busam, S. and Dullenkopf, K., 2006, "Influence of Operating Condition and Geometry on the Oil Film Thickness in Aero-Engine Bearing Chambers", ASME Journal of Engineering for Gas Turbines and Power, Vol. 128, pp. 103-110.

[6] Kurz, W., Dullenkopf, K., and Bauer, H.-J., 2012, "Influences on the oil split between the offtakes of an aero-engine bearing chamber", Proceedings of ASME Turbo Expo 2012, Copenhagen, Denmark, June 2012, GT2012-69412.

[7] Kurz, W., Dullenkopf, K., and Bauer, H.-J., 2012, "Capacitive film thickness measurements in a ventless aero-engine bearing chamber – influence of operating", Proceedings of ASME Turbo Expo 2013, San Antonio, Texas, USA, June 2013, GT2013-94973.

[8] Kurz, W., Bauer, H.-J., 2014, "An approach for predicting the flow regime in an aero engine bearing chamber", Proceedings of ASME Turbo Expo 2014, Düsseldorf, Germany, June 2014, GT2014-26756.

[9] Glahn, A., Busam, S., and Wittig, S., 1997, ‘‘Local and Mean Heat Transfer Coefficients along the Internal Housing Walls of Aero Engine Bearing Chambers,’’ ASME Paper 97-GT-261.

[10] Busam, S., Glahn, A., and Wittig, S., 2000, “Internal Bearing Chamber Wall Heat Transfer as a Function of Operating Conditions and Chamber Geometry”, ASME Journal of Engineering for Gas Turbines and Power, Vol. 122, pp. 314-320.

[11] Yuan Xichuan, Guo Hui and Wang Liangyun, 2011, “Experiment Study of Heat Transfer in Aeroengine Bearing Chambers”, Applied Mechanics and Materials, Trans Tech Publications, Switzerland, Vol 86 (2011), pp. 448-453.

[12] Zhenxia Liu, Fei Zhang, 2017, “The numerical simulation and experimental study on aero-engine bearing cavity wall heat transfer”, ISABE-2017-21379.

[13] Farral, M., Simmons, K., Hibberd, S., and Gorse, P., 2004, “A Numerical Model for Oil Film Flow in an Aero-engine Bearing Chamber and Comparison with Experimental Data,” Proceedings of ASME Turbo Expo 2004, Vienna, Austria, June 2004, GT2004-53698.

[14] Kakimpa, B., Morvan, H. P. and Hibberd, S., 2015, “Thin-film flow over a rotating plate: an assessment of the suitability of VOF and Eulerian Thin-Film Methods for the numerical simulation of isothermal thin-film flows”, Proceedings of ASME Turbo Expo 2015, Montréal, Canada, June 2015, GT2015-43506.

[15] Kakimpa, B., Morvan, H. P. and Hibberd, S., 2016, “The numerical simulation of multi-scale oil films using coupled VOF and Eulerian thin-film models”, Proceedings of ASME Turbo Expo 2016, Seoul, South Korea, June 2016, GT2016-56747.

[16] Bristot, A., Morvan, H., Simmons, K., 2016, “Evaluation of a volume of fluid CFD methodology for the oil film thickness estimation in an aero-engine bearing chamber”. Proceedings of ASME Turbo Expo 2016, Seoul, South Korea, June 2016, GT2016-56237.

[17] Adeniyi, A. A, Chandra, B., Simmons, **K**., 2017, “Computational study of a customised shallow-sump aero-engine bearing chamber with inserts to improve oil residence volume”, Proceedings of ASME Turbo Expo 2017, Charlotte, NC, USA, June 2017, GT2017-64410.

[18] Singh, K., Sharabi, M., Ambrose, S., Eastwick, C., Jefferson-Loveday, R., Cao, J., Jacobs, A., 2019, “Assessment of an enhanced thin film model to capture wetting and drying behavior in an aero-engine bearing chamber”, Proceedings of ASME Turbo Expo 2019, Phoenix, Arizona, USA, June 2019, GT2019-91323.

[19] Singh, K., Sharabi, M., Ambrose, S., Eastwick, C., Jefferson-Loveday, R., 2019, “Prediction of film thickness of an aero-engine bearing chamber using coupled VOF and thin film model”, Proceedings of ASME Turbo Expo 2019, Phoenix, Arizona, USA, June 2019, GT2019-91314.

[20] Shchukin, V. K. Teploobmen i gidrodinamika vnutrennikh potokov v polyakh massovykh sil [Heat transfer and hydrodynamics of internal flows in the fields of mass forces]. Moscow, Engineering Publ., 1970. 332 p

[21] Demidovich, V. M., 1978, Study of the Thermal Condition of Gas Turbine Bearings (Moscow: Mashinostroenie).

[22] Flouros, M., 2006, “Correlations for heat generation and outer ring temperature of high speed and highly loaded ball bearings in an aero-engine”, Aerospace Science and Technology, 10, pp. 611-617.

[23] Gupta, P. K., Taketa, J. I., & Price, C. M., 2019, “Thermal interactions in rolling bearings”, Proceedings of the Institution of Mechanical Engineers, Part J: Journal of Engineering Tribology, pp. 1-21.

[24] ANSYS Help. Release 2020 R1.

[25] Moran, K., Inumaru, J. and Kawaji, M. 2002, “Instantaneous hydrodynamics of a laminar wavy liquid film”, nternational Journal of Multiphase Flow, Vol. 28 pp. 731–755